RSC Advances

ROYAL SOCIETY OF CHEMISTRY

www.rsc.org/advances

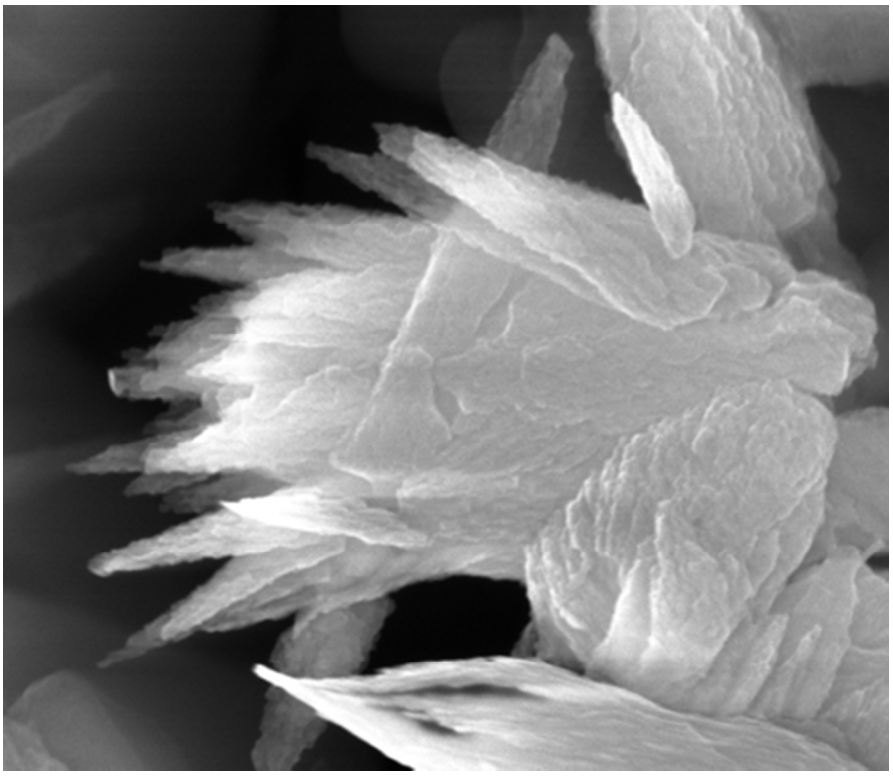

37x32mm (300 x 300 DPI)

Journal Name

RSCPublishing

ARTICLE

Hydrothermal synthesized CuO based volatile organic compound gas sensor

Cite this: DOI: 10.1039/xoxxoooooox

Shufeng Xia,[ab] Huichao Zhu,[*ab] Haitao Cai,[a] Jiaqi Zhang,[a] Jun Yu[ab] and Zhen'an Tang[*ab]

Received 22th August 2014,
Accepted ooth August 2014

DOI: 10.1039/xoxxoooooox

www.rsc.org/advances

In present work, single-phase CuO particles were synthesized by hydrothermal method and characterized by SEM, TEM and XRD. The gas sensing properties of CuO based sensor to some representative flammable VOC gases such as ethanol, isopropanol, acetone, benzene, para-xylene and decane were investigated. The sensor resistance increased when exposed to these flammable analytes, as well as when the concentration of oxygen in air decreased. That phenomenon is attributed to the surface accumulation conduction mechanism of p-type metal oxide semiconductor, when negatively charged surface oxygen desorbs from the surface of CuO and release electrons back to CuO bulk. According to our research, the detection limit of the CuO based sensor to decane was better than 1ppm, which indicated the potential applications of CuO based sensors in detecting low concentration decane.

1. Introduction

Semiconductor metal oxide based gas sensors have been extensively investigated for detection of hazardous, humid, flammable or toxic gases, due to the low cost, flexibility and simplicity in their production and use, and large number of detectable gases.[1] Many n-type semiconducting metal oxides, such as SnO_2,[2] ZnO,[3] WO_3,[4] Fe_2O_3[5] and MoO_3,[6] have been thoroughly researched due to their extensive sensing performance. Recent years, increasing interests have been focused on p-type semiconducting metal oxides such as CuO,[7] Co_3O_4,[8] MnO_x[9] and NiO,[10] due to their extremely sensitivity to the hazard gas such as H_2S,[11] or better selectivity to some VOCs.[12] In addition, comparing with n-type metal oxide semiconductor sensors, p-type ones typically have much lower resistance, e.g. several hundreds of ohms at the working temperature above 200°C, and provide better signal noise ratio, also simplify the design of associate electronic circuits.

CuO is known as an eco-friendly and thermostable p-type semiconductor with a band gap of ~1.3eV because of presence of acceptors levels attributed to copper vacancies. It is believed to be an excellent candidate for long-term stable and low-power consumption sensing devices. There have been some reports on CuO nanoparticles,[13] nanowires,[14] nanorods,[15] nanoribbons,[16] nanosheets[17] and microspheres,[18] towards a few target gases such as NO_2, H_2S, NH_3, CO and C_2H_5OH, in the working temperature ranging from 200°C to 400°C. Researchers are still working hard in improving these gas sensor's sensitivity, selectivity, stability, speed of response and linearity.

In this work, single-phase p-type CuO particles were synthesized by low temperature, normal pressure hydrothermal method (i.e. water bath method). Ethanol, Isopropanol (IPA), acetone, benzene, para-xylene (PX) and decane are representative flammable volatile organic compounds (VOCs) widely used in modern chemistry industry. The sensing properties to these VOC gases were investigated by varying the gas category and concentration. According to our research, the as-made CuO based VOC sensors work at lower temperature and have a better sensitivity, comparing to some recent reports towards ethanol[19] and IPA.[20] Furthermore, in this work, the detection limit of the CuO based sensor to decane was better than 1ppm, which indicated the potential applications in detecting low concentration decane, and there're few reports on this.

2. Experimental

2.1 Material preparation

The CuO particles were synthesized as following steps. All the chemical reagents used were analytical grade. The synthesis was conducted by the thermal decomposition of a Cu^{2+} amino complex with reagent-grade chemicals. Copper (II) nitrate hemipentahydrate ($Cu(NO_3)_2{\cdot}2.5H_2O$), methenamine ($(CH_2)_6N_4$) and deionized water were employed in the synthesis process. Methenamine, a water-soluble nontoxic and non-ionic tetradentate cyclic tertiary amine, was chosen to comply simultaneously with the precipitation of the divalent transition metal ion Cu^{2+} and the nucleation growth to its stable oxide form, CuO. An equimolar (0.1 M) aqueous solution of $Cu(NO_3)_2{\cdot}2.5H_2O$ and $(CH_2)_6N_4$ was separately prepared and mixed in a glass bottle with a plastic (PP) screw cap (the cap is not fastened to keep normal pressure). The bottle was heated at 100°C for 6 hours in a laboratory water bath. Subsequently, the

[a] College of Electronic Science and Technology, Dalian University of Technology, Dalian 116023, Liaoning, P. R. China.
[b] The Key Laboratory for Integrated Circuits Technology of Liaoning Province, Dalian 116023, Liaoning, P. R. China.
Email: zhuhuichao@dlut.edu.cn; tangza@dlut.edu.cn

homogeneous particles were thoroughly washed with deionized water to remove any contamination complex.[21]

2.2 Sensor device preparation

The prepared powder was mixed with terpineol uniformly to improve the adhesion between the material and the substrate. The paste was brushed onto an alumina substrate with eight pairs of gold interdigital electrodes, and the width and clearance of the electrodes were both 250μm. Then the sensor device was slowly heated to 200°C and held for 2 hours in a tubular furnace to make the paste dry out. Finally, the device was annealed in air at 500°C for 5 hours, then cooled down to room temperature naturally.

The crystalline structure of the as grown CuO particles was analyzed by an X-ray powder diffractometer (XRD, "Bruker D8 ADVANCE", Cu Kα radiation with λ=1.5406Å). The goniometer scanning rate was 0.4° min^{-1}. The samples were pressed onto an alumina substrate before scanning. The morphology and microstructure of the as grown CuO particles were investigated through a scanning electron microscope (SEM, "JEOL JSM-6700F") and a high-resolution transmission electron microscope (HRTEM, "Tecnai G^2 F20 S-TWIN", working at 200 kV with a LaB_6 filament).

2.3 Gas sensor test measurements

A specially made clamp was introduced to keep good contact between sensor and signal wires at high temperature. As shown in Fig.1, A to C are alumina ceramic plates with 0.95mm thickness. Two gold wires (S1 and S2) with 0.5mm diameter pass through small holes pre-drilled on plate B and act as electrical contacts. Sensor device is fitted into a gap pre-milled on plate C. Sensors are very easy to be replaced, eliminating the traditional high-temperature and time-consuming procedure of soldering gold wires to electrodes. Further, more plates can be stacked up as required, to test multiple sensors simultaneously.
Dynamic gas sensing measurements were performed in a computer controlled automatic testing system shown in Fig. 2. Synthetic air (oxygen, nitrogen mixture without humidity) was used as reference gas, also carrier gas, and passed through four computer driven mass-flow controllers (MFC). Channel 4 was used to generate bubbles and drive analyte vapor out of a gas washing bottle. The gas washing bottle with analyte liquid were preserving 0°C in ice-water mixture to obtain desired saturated vapor pressure (as listed in Table 1). Channel 1 to 3 were combined and used to dilute analyte vapor from channel 4. The sensor signal is strongly temperature dependent, so it's important to stabilize gas flow rate to prevent temperature fluctuations, thus avoiding spikes on resistance curve. In this system, the total flow rate of 4 MFCs was kept stable at 300sccm. That implies if the flow rate of channel 4 is increased, the flow rate of other 3 channels must be decreased to keep the total flow rate invariable at 300 sccm, and vice versa.

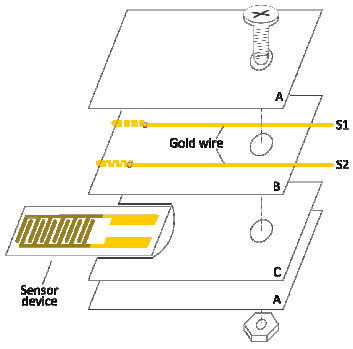

Fig. 1 Assembly of the high temperature clamp

Prior to test, the sensor was preheated at 300°C for 1 hour for stable references, then all measurements were performed at 230°C. The sensor was exposed to analyte gas with desired concentration for 2min and then to reference gas for 4min. Agilent B1500A semiconductor device analyzer was employed to record the sensor's resistance under the influence of different analyte gases and different concentrations. Constant current measurement mode was used with a test current of 0.5mA. The response of the sensor (S) is defined as: S = Rg/Ra, where Rg and Ra are the resistances of the sensor in test gases and in air (reference gas), respectively.

According to the "Daltons law of partial pressures", the concentration of analyte vapor in the gas washing bottle equals to the ratio of its saturated vapor pressure (SVP) to standard atmospheric pressure (ATM, 101.325kPa). The final diluted analyte concentration in test gas (con) can be calculated by equation 2.1, where V_4 is the flow rate of channel 4, and V_{all} is

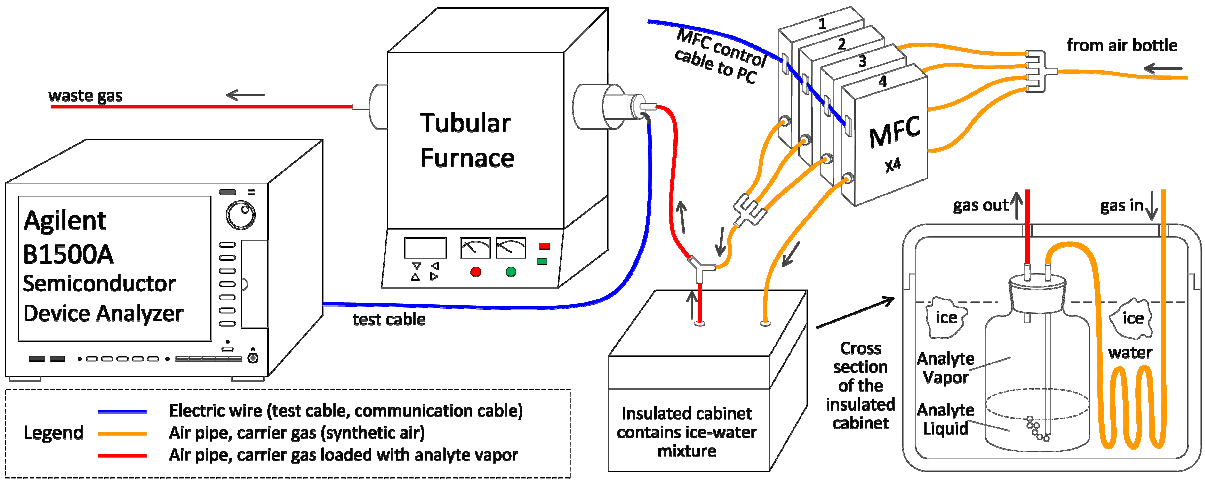

Fig. 2 Gas transport and sensor measurement system

the total flow rate of all four channels (i.e. 300 sccm); k is developed to denote the concentration by per sccm of channel 4, as listed for different analytes in Table 1. For example, the k for ethanol is 52.26ppm/sccm at 0°C and standard atmosphere, and if the flow rate of channel 4 (in curves shown in Fig.7) is 3sccm, then the analyte concentration in final test gas can be calculated simply as 52.26×3≈157ppm.

$$con = \frac{V_4}{V_{all}} \cdot \frac{SVP}{ATM} = V_4 \cdot \left(\frac{1}{V_{all}} \cdot \frac{SVP}{ATM} \right) = V_4 \cdot k \qquad (2.1)$$

According to the "Antoine equation", saturated vapor pressure decreases when temperature drops. To obtain low vapor concentrations, analytes were preserving 0°C in an ice-water mixture environment, as shown in Fig. 2. Saturated vapor pressures of the analytes were calculated using an online calculator[22] as shown in Table 1. The Para-xylene (PX) was tested at room temperature (22°C) due to it has a freezing point of 13.2°C, and would freeze at 0°C.

Table 1 Saturated vapor pressure and concentration of the tested analysts at standard atmosphere

Analytes	Temp. (°C)	Saturated vapor pressure (kPa)	k (ppm sccm^{-1})
Ethanol	0	1.5887	52.26
Isopropanol	0	0.9609	31.61
Acetone	0	9.3576	307.84
Benzene	0	3.5118	115.53
Para-xylene	22	0.9791	32.21
Decane	0	0.0227	0.7467

3. Results and discussion

3.1 XRD, SEM and HRTEM analysis

Fig. 3 shows XRD patterns of CuO particles. All the diffraction peaks can be readily indexed by the monoclinic tenorite CuO structure with lattice constant a=4.69Å, b=3.43Å, c=5.13Å (JCPDS: 45-0937), indicating a single phase of monoclinic CuO. The diffraction peaks located at 2θ angle of 32.5°, 35.5°, 38.8°, 48.7°, 58.3°, 61.5°, 66.5°, 68.1°, 75.0° were indexed to CuO (−110), (002), (111), (−202), (202), (−113), (−311), (−220) and (004), respectively.[23] The peaks observed at 35.1°, 43.3°, etc., were due to the alumina (Al_2O_3) substrate (JCPDS: 46-1212). The most intense (002) peak at 2θ=35.5° was partially overlapped with a signal related to Al_2O_3 substrate. No peaks for Cu_2O or other impurities could be detected. The average crystallite size of the synthesized CuO particles (30nm) can be roughly estimated by Scherrer's formula: D=κλ/βcosθ, where β is the full width at half maximum (FWHM) of a diffraction peak in radian (0.004957 rad), θ is the diffraction angle in degree (17.75°), λ is the X-ray wavelength (0.154 nm), and κ (0.9) is the Scherrer's constant of the order of unity for a usual crystal.[24]

The SEM image of the as grown CuO particles is shown in Fig. 4. These featherlike particles have typical dimensions of 200-800 nm in length, 20-100 nm in width, and were assembled to multi-layered structures. Rough surface is a dominant feature, which provides high surface-to-volume ratio and a great number of active sites for gas adsorption. The formation of irregular bumpy surfaces on the CuO particles is attributed to the vibrant hydrothermal process and relief of stress generated during nucleation. The stress may come from recrystallization or nonstoichiometric formation process. During the oxidation process, the natural nonstoichiometric defects altered the electrical properties of the CuO particles, causing a metal deficient p-type semiconducting behavior.[11, 25, 26]

The detailed structure of the as grown CuO particles was characterized by a HRTEM. Fig. 5 shows a typical TEM and HRTEM image of the sample, along with the selected area electron diffraction (SAED) pattern. In Fig. 5(b), the distance

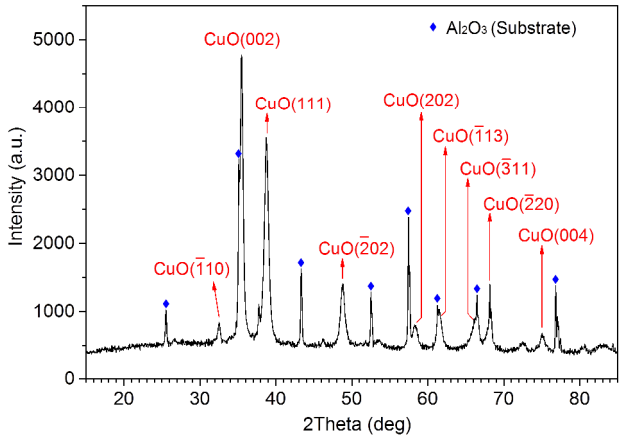

Fig. 3 The XRD pattern of as grown CuO particles

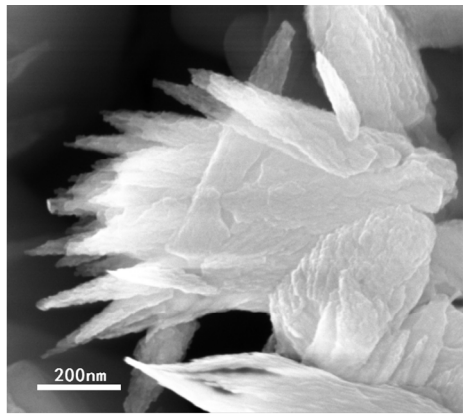

Fig. 4 The SEM image of as grown CuO particles

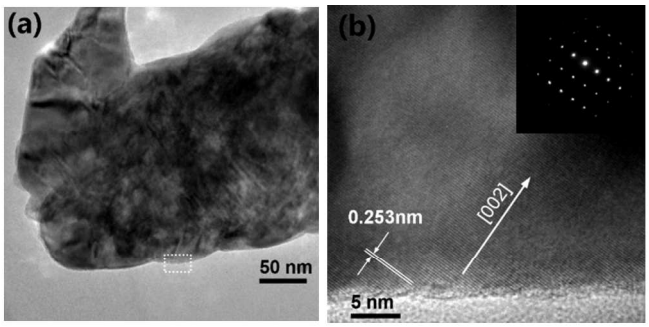

Fig. 5 The HRTEM image and SAED pattern

between adjacent planes is measured to be about 0.253nm by FFT method. This value matched the lattice spacing of the {002}c plane of CuO according to (JCPDS: 45-0937). It can be concluded from the HRTEM characterization that the particles grow along a direction parallel to [002]. The inset in Fig. 5(b) is the SAED pattern which indicates that it is single crystalline.

3.2 Response and recovery characteristics

Gas molecules adsorbed on the surface of CuO particles have remarkable tuning effects on the electrical properties due to their high surface-to-volume ratio. The sensing mechanism of CuO particles originates from the interaction between the analyte gases and the pre-adsorbed oxygen on the CuO surfaces, as shown in the upper part of Fig.6 (a).[27] The pre-adsorbed oxygen may establish forms of O^- and/or O^{2-} at the CuO surface through charge exchange interactions with CuO following equations (3.1–3.4).[24] When such CuO is exposed to reductive molecules, taking ethanol as example, the adsorbed reductive molecules interact with the pre-adsorbed oxygen as shown in equations (3.5–3.7). The reactions between the reductive molecules and the pre-adsorbed O^- or O^{2-} release free electrons and neutralize the holes (equation 3.8), the majority carrier in p-type CuO. This compensation results in a decrease in the holes in CuO, and consequently, an increase in sensor resistance. Note that the oxygen molecules are continuously supplied from the dilute gas (synthetic air) and are adsorbed on the CuO surface while the interaction with reductive molecules to desorption from the surface, with the trend towards an equilibrium state.[24] When the concentration of reductive analyte is decreased, more oxygen molecules in air will adsorb on the surface of CuO, and the capture of electrons through the processes indicated in equations (3.1–3.4) will reduce the sensor resistance towards the initial stable surface state of CuO.

$$O_2(gas) \leftrightarrow O_2(ads) \quad (3.1)$$

$$O_2(ads)+e^- \leftrightarrow O_2^-(ads) \quad (3.2)$$

$$O_2^-(ads)+e^- \leftrightarrow 2O^-(ads) \quad (3.3)$$

$$O^-(ads)+e^- \leftrightarrow O^{2-}(ads) \quad (3.4)$$

$$C_2H_6O(gas) \leftrightarrow C_2H_6O(ads) \quad (3.5)$$

$$C_2H_6O(ads)+6O^-(ads) \leftrightarrow 2CO_2+3H_2O+6e^- \quad (3.6)$$

$$C_2H_6O(ads)+6O^{2-}(ads) \leftrightarrow 2CO_2+3H_2O+12e^- \quad (3.7)$$

$$e^-+h^{\square} \leftrightarrow NULL \quad (3.8)$$

The bottom of the conduction band of CuO is about 4.07eV below the vacuum energy, and its band gap is reported to be 1.36eV.[28] Adsorbed oxygen with chemical potential of about 5.7eV[29] below the vacuum energy will form acceptor levels near the valence band at the surface. As mentioned above, the electrons are trapped by the adsorbed oxygen, and the energy band also bends upwards at the surface, which leads to the formation of an accumulation layer for CuO with majority carriers of holes. Trapping of the electrons leaves more holes available near the surface. During this process, the band bends between the particles due to the surface accumulation will act as no barrier for the holes, the majority carriers of p-type CuO, as shown in lower part of Fig.6 (a).[27] Accordingly, the conductivity in the surface space charge layer increases in comparison with the one in the bulk, and that means the conduction in the sensing layer of p-type MOX will take place quite differently than in the case of n-type MOX. The n-type MOX has an electron depletion layer on the surface and the contact barriers play a very important role in controlling the resistance.[29-32]

Bârsan et al.[33] suggested the surface accumulation conduction model for p-type MOX, instead of the grain boundary model for n-type MOX, using a cube with an edge size larger than twice of the thickness of the charge accumulation layer (i.e. twice the Debye length L_D). It's considered when the contact size is ten times higher than L_D, the contact size hardly influences the gas response, and the contacts between particles do not contribute much to the resistance of the device, which can account for the low resistance of the p-type device. In p-type MOX, the holes mainly flow through the surface charge accumulation layer (CAL) "parallel" to the surface, and also through the bulk. When the particle size is greater than twice the thickness of the CAL, an electronic core-shell configuration is established with a p-semiconducting shell and a resistive core.[34] How large the contribution of the bulk component to the overall resistance

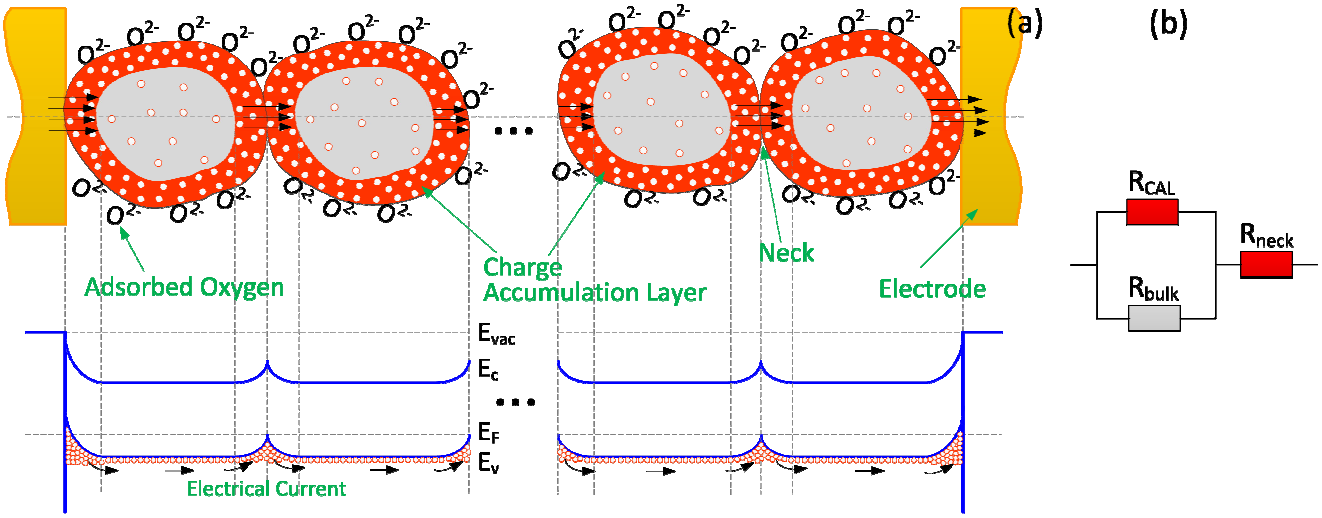

Fig. 6 Illustration of (a) conduction processes in the sensing layer and the corresponding energy bands representation for p-type metal oxide semiconductor with charge accumulation layer and (b) the DC equivalent circuit of one particle

through the sensing layer is, depends on the actual sensing layer morphology. Obviously, the large the grains are, when compared to the thickness of the accumulation layer, the large the bulk contribution would be, and by that making the surface effects, i.e. the gas sensing, less important. When performing DC test, the parasitic capacitance can be ignored, thus the equivalent electronic circuit is as shown in Fig.6 (b).[35] The conduction is determined by parallel competition between the conduction along the conductive shell and the resistive core in addition to the series neck resistance. Under this condition, as suggested by Pokhrel et al.,[36] a high response to reducing gas is relatively difficult to accomplish in p-type MOX even with the huge surface changes due to this conduction mechanism.

The dynamic response and recovery characters of one and the same sensor were tested to different flammable volatile organic compounds (VOCs): ethanol, isopropanol (IPA), acetone, benzene, para-xylene (PX), and decane, as shown in Fig. 7. The baseline resistance of the sensor (Ra) was in the range of 140 – 200 ohm. As mentioned above, when exposed to reducing gases, the adsorbed oxygen (O^-, O^{2-}) on CuO surface will react with the analyte molecules and release electrons to the conduction band. This leads to the decrease of carrier holes in

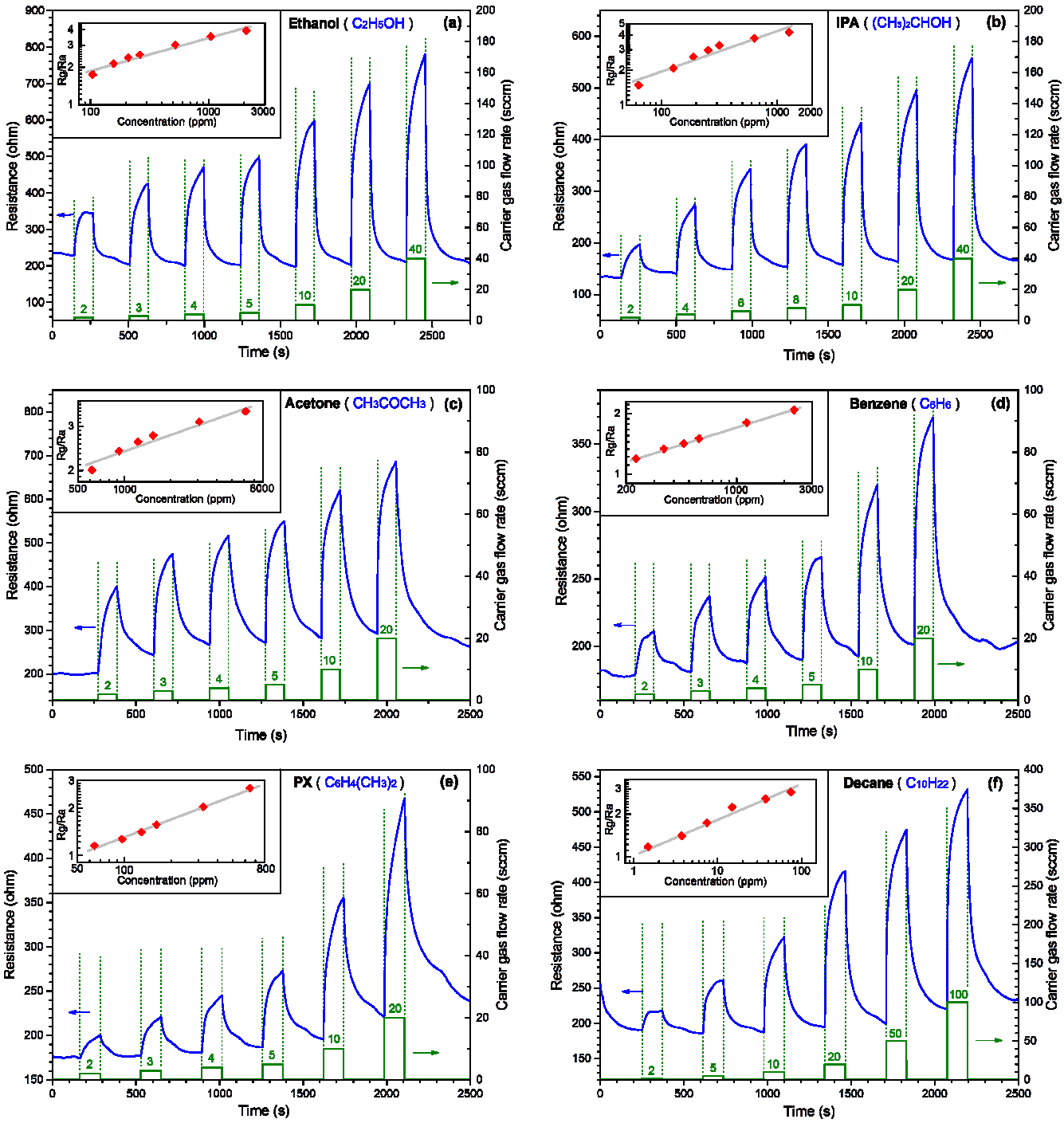

Fig. 7 Dynamic response/recovery plots of CuO to different analytes at 230°C

the surface charge layer and the increase of sensor resistance. After the analyte gas flow is stopped, the resistance returns towards the baseline value due to the trapping of electrons of the oxygen re-adsorption process.

The sensor response to different gas concentrations was also investigated for every analyte. No clear evidence of saturation phenomena was observed at relative high concentration (e.g. 6000ppm for acetone). In previous reports,[7, 16, 29] the CuO nanosystems response increased proportionally to different target gas concentration, especially at low concentrations.[7, 11]

In this work, the sensitivity of the as-made single phase CuO particle based sensor to ethanol at 230°C was S=2.37@210ppm and S=3.53@1050ppm, which was better than some recent reports (single crystal CuO nanowires, S=1.35@250ppm and S=1.8@1000ppm, at 400°C).[19] Again, the sensitivity of this CuO particle based sensor to IPA was S=2.6@190ppm, which was better than some reports (CuO nanotube, S=1.13@200ppm, at 300°C).[20] The CuO based sensor in this work works at lower temperature and has better performance than those works.

In present work, the experimental response-concentration relation follows equation (4.1), the typical formula reported for semiconductor metal oxide-based gas sensors,[29, 37-39] where S and C denote the response values and analyte concentrations respectively, while K and N are constants for a certain material. Equation (4.2) is the logarithmic form of equation (4.1), where lgS and lgC have a linear relation.

$$S = K \cdot C^N \tag{4.1}$$

$$\lg S = \lg K + N \cdot \lg C \tag{4.2}$$

Sensor response S (Rg/Ra) and gas concentration C were drawn in logarithmic coordinates in the insets of Fig. 7 for every analyte, and approximate linear relations between lgS and lgC could be observed. In addition, it could be discovered from Fig.7 (f) that the as grown CuO particles showed better sensitivity to decane than to other analytes, and the detection limit was better than 1ppm. Further studies on other hydrocarbon analytes may be established.

A further experiment was carried out to investigate the affections of oxygen concentration variations on the electrical properties of CuO particles. Synthetic air (21% oxygen and 79% nitrogen) and pure nitrogen were mixed dynamically with different flow rate to obtain different oxygen concentrations in test gas from 21% to 0%. The resistance of the sensor was measured in the test gas. Ra is the baseline resistance measured in synthetic air, Rg is that measured in the test gas. As shown in Fig. 8, in the first 8 pulses, the sensor was exposed in the test gas for 3min and then exposed in synthetic air for 6min. In the last pulse, the sensor's response approached a saturate state after exposed in 0% oxygen (pure nitrogen) for more than 30min. The resistance increased as the oxygen concentration decreased, and recovered as the oxygen concentration returned to normal. Such phenomenon can be attributed to the effects of oxygen partially desorption and re-adsorption, which influenced the thickness of surface accumulation layer and resulted in the change of resistance. It took the resistance more time to reach saturate state in low oxygen concentration atmosphere than in high oxygen concentration atmosphere, and the recovery time was shorter than the time reaching saturate. Such phenomena indicated that oxygen adsorbed on the CuO surface more easily than it desorbed from the CuO surface. The fact of the saturation resistance in pure nitrogen atmosphere reached a finite value about two folds of the resistance in air, indicated that the oxygen partially desorbed from the surface of CuO in this situation.

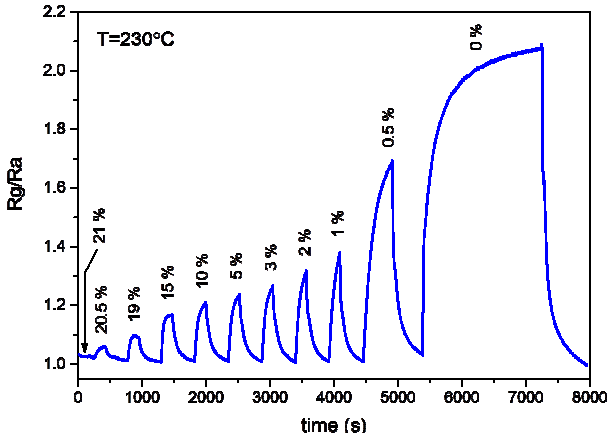

Fig. 8 Influence of oxygen concentration to sensor response

Conclusions

In summary, CuO particles were synthesized by hydrothermal method. The sensing properties under different flammable VOC gases and different concentrations were investigated. A surface accumulation conduction model for p-type metal oxide semiconductors was used to explain the sensing mechanism. The CuO based sensor showed better sensitivity to decane, and the detection limit for decane was lower than 1ppm. It may have the potential to be used as decane or other hydrocarbon gas detectors. The sensor responses to oxygen concentration were also investigated and the CuO based sensor showed large response to the decrease of oxygen concentration. It indicated that in practical application that oxygen was consumed and oxygen concentration decreased, this response character to oxygen concentration should be considered.

Acknowledgements

This work was supported by the National Natural Science Foundation of China (No. 61107028, 61131004, 61274076).

Notes and references

1. N. Barsan, D. Koziej and U. Weimar, *Sensors and Actuators B: Chemical*, 2007, **121**, 18-35.
2. T. Itoh, T. Nakashima, T. Akamatsu, N. Izu and W. Shin, *Sensor Actuat B-Chem*, 2013, **187**, 135-141.
3. H. Yue and A. H. Jayatissa, *Appl. Surf. Sci.*, 2014, **309**, 46-53.
4. X. Bai, H. M. Ji, P. Gao, Y. Zhang and X. H. Sun, *Sensor Actuat B-Chem*, 2014, **193**, 100-106.
5. H. Shan, C. Liu, L. Liu, S. Li, L. Wang, X. Zhang, X. Bo and X. Chi, *Sensor Actuat B-Chem*, 2013, **184**, 243-247.
6. P. Song, Q. Wang, J. Li and Z. Yang, *Sensor Actuat B-Chem*, 2013, **181**, 620-628.
7. Y. Zhang, X. L. He, J. P. Li, H. G. Zhang and X. G. Gao, *Sensor Actuat B-Chem*, 2007, **128**, 293-298.
8. S. Liu, Z. Wang, H. Zhao, T. Fei and T. Zhang, *Sensor Actuat B-Chem*, 2014, **197**, 342-349.
9. D. Jung, Y. Yoon and G. S. Lee, *Chemical Physics Letters*, 2013, **577**, 96-101.
10. H. Steinebach, S. Kannan, L. Rieth and F. Solzbacher, *Sensor Actuat B-Chem*, 2010, **151**, 162-168.

11. X. Li, Y. Wang, Y. Lei and Z. Gu, *RSC Advances*, 2012, **2**, 2302.
12. L. L. Wang, J. A. Deng, Z. Lou and T. Zhang, *Sensor Actuat B-Chem*, 2014, **201**, 1-6.
13. B. J. Hansen, N. Kouklin, G. H. Lu, I. K. Lin, J. H. Chen and X. Zhang, *J Phys Chem C*, 2010, **114**, 2440-2447.
14. S. Steinhauer, E. Brunet, T. Maier, G. C. Mutinati, A. Kock, O. Freudenberg, C. Gspan, W. Grogger, A. Neuhold and R. Resel, *Sensor Actuat B-Chem*, 2013, **187**, 50-57.
15. H. Kim, C. Jin, S. Park, S. Kim and C. Lee, *Sensor Actuat B-Chem*, 2012, **161**, 594-599.
16. X. Gou, G. Wang, J. Yang, J. Park and D. Wexler, *Journal of Materials Chemistry*, 2008, **18**, 965-969.
17. M. Faisal, S. B. Khan, M. M. Rahman, A. Jamal and A. Umar, *Materials Letters*, 2011, **65**, 1400-1403.
18. Z. Yang, H. Xiuli, L. Jianping, Z. Huigang and G. Xiaoguang, *Sensors & Actuators: B. Chemical*, 2007, **128**, 293-298.
19. D. Le Duy, L. Dang Thi Thanh, D. Nguyen Van, H. Nguyen Duc and H. Nguyen Van, *Physica E: Low-dimensional Systems and Nanostructures*, 2014, **58**, 16-23.
20. H.-T. Hsueh, S.-J. Chang, F.-Y. Hung, W.-Y. Weng, S. P. Chang, T. J. Hsueh, C.-L. Hsu and B.-T. Dai, *Ieee Sens J*, 2011, **11**, 3276-3282.
21. M. H. Chen, H. C. Zhu, X. G. Li, J. Yu, H. T. Cai, X. T. Quan, K. L. Wang and J. Q. Zhang, *J Nanomater*, 2014, **2014**, 461269.
22. www.envmodels.com, *Vapour pressure calculation*, http://www.envmodels.com/freetools.php?menu=pression&lang=en, Accessed 01 July, 2014.
23. H. T. Hsueh, T. J. Hsueh, S. J. Chang, F. Y. Hung, T. Y. Tsai, W. Y. Weng, C. L. Hsu and B. T. Dai, *Sensor Actuat B-Chem*, 2011, **156**, 906-911.
24. N. D. Hoa, S. Y. An, N. Q. Dung, N. V. Quy and D. Kim, *Sensor Actuat B-Chem*, 2010, **146**, 239-244.
25. N. Birks, G. H. Meier and F. S. Pettit, *Introduction to the High Temperature Oxidation of Metals*, 2nd edn., Cambridge University Press, 2009.
26. E. G. Seebauer and M. C. Kratzer, *Charged Semiconductor Defects: Structure, Thermodynamics and Diffusion*, Springer London Ltd, 2010.
27. M. Huebner, C. E. Simion, A. Tomescu-Stanoiu, S. Pokhrel, N. Barsan and U. Weimar, *Sensor Actuat B-Chem*, 2011, **153**, 347-353.
28. F. P. Koffyberg and F. A. Benko, *Journal of Applied Physics*, 1982, **53**, 1173-1177.
29. C. Wang, X. Q. Fu, X. Y. Xue, Y. G. Wang and T. H. Wang, *Nanotechnology*, 2007, **18**, 145506.
30. Q. Wan, Q. H. Li, Y. J. Chen, T. H. Wang, X. L. He, J. P. Li and C. L. Lin, *Applied Physics Letters*, 2004, **84**, 3654-3656.
31. P. Feng, Q. Wan and T. H. Wang, *Applied Physics Letters*, 2005, **87**, 213111.
32. Y. J. Chen, X. Y. Xue, Y. G. Wang and T. H. Wang, *Applied Physics Letters*, 2005, **87**, 233503.
33. N. Barsan, C. Simion, T. Heine, S. Pokhrel and U. Weimar, *J Electroceram*, 2010, **25**, 11-19.
34. J. W. Yoon, H. J. Kim, H. M. Jeong and J. H. Lee, *Sensor Actuat B-Chem*, 2014, **202**, 263-271.
35. J. W. Yoon, J. K. Choi and J. H. Lee, *Sensor Actuat B-Chem*, 2012, **161**, 570-577.
36. S. Pokhrel, C. E. Simion, V. Quemener, N. Barsan and U. Weimar, *Sensor Actuat B-Chem*, 2008, **133**, 78-83.
37. D. Barreca, E. Comini, A. P. Ferrucci, A. Gasparotto, C. Maccato, C. Maragno, G. Sberveglieri and E. Tondello, *Chem Mater*, 2007, **19**, 5642-5649.
38. R. W. J. Scott, S. M. Yang, G. Chabanis, N. Coombs, D. E. Williams and G. A. Ozin, *Adv Mater*, 2001, **13**, 1468-1472.
39. M. Graf, D. Barrettino, M. Zimmermann, A. Hierlemann, H. Baltes, S. Hahn, N. Barsan and U. Weimar, *Ieee Sens J*, 2004, **4**, 9-16.